Carbon-rich icosahedral boron carbides beyond B_4C and their thermodynamic stabilities at high temperature and pressure from first principles

A. Ektarawong,[1,*] S. I. Simak,[2] and B. Alling[1,3]

[1]*Thin Film Physics Division, Department of Physics, Chemistry and Biology (IFM), Linköping University, SE-581 83 Linköping, Sweden*

[2]*Theoretical Physics Division, Department of Physics, Chemistry and Biology (IFM), Linköping University, SE-581 83 Linköping, Sweden*

[3]*Max-Planck-Institut für Eisenforschung GmbH, D-40237 Düsseldorf, Germany*

(Received 4 June 2016; published 10 August 2016)

We investigate the thermodynamic stability of carbon-rich icosahedral boron carbide at different compositions, ranging from B_4C to B_2C, using first-principles calculations. Apart from B_4C, generally addressed in the literature, $B_{2.5}C$, represented by $B_{10}C_2^p$(C-C), where C^p and (C-C) denote a carbon atom occupying the polar site of the icosahedral cluster and a diatomic carbon chain, respectively, is predicted to be thermodynamically stable under high pressures with respect to B_4C as well as pure boron and carbon phases. The thermodynamic stability of $B_{2.5}C$ is determined by the Gibbs free energy G as a function of pressure p and temperature T, in which the contributions from the lattice vibrations and the configurational disorder are obtained within the quasiharmonic and the mean-field approximations, respectively. The stability range of $B_{2.5}C$ is then illustrated through the p-T phase diagrams. Depending on the temperatures, the stability range of $B_{2.5}C$ is predicted to be within the range between 40 and 67 GPa. At $T \gtrsim 500$ K, the icosahedral C^p atoms in $B_{2.5}C$ configurationally disorder at the polar sites. By investigating the properties of $B_{2.5}C$, e.g., elastic constants and phonon and electronic density of states, we demonstrate that $B_{2.5}C$ is both mechanically and dynamically stable at zero pressure, and is an electrical semiconductor. Furthermore, based on the sketched phase diagrams, a possible route for experimental synthesis of $B_{2.5}C$ as well as a fingerprint for its characterization from the simulations of x-ray powder diffraction pattern are suggested.

DOI: 10.1103/PhysRevB.94.054104

I. INTRODUCTION

Due to its outstanding properties, for example high chemical stability, high hardness, low wear coefficient, high melting point, and low density, boron carbide is a promising material for several technological applications [1–6]. Boron carbide is categorized as an icosahedral boron-rich solid. Its crystal structure can be described by 12-atom icosahedra, placed at vertices of a rhombohedral unit cell with $R\bar{3}m$ space group, and connecting to 3-atom inter-icosahedral chains, residing in the interstices between the icosahedra along the [111] direction of the rhombohedron [7–10]. Each icosahedron is composed fundamentally of two crystallographic sites, termed "polar" and "equatorial." In addition, each icosahedron is linking to six neighboring icosahedra to form the icosahedral network through the inter-icosahedral bonds between the polar atoms, while the inter-icosahedral chains are linking to the surrounding icosahedra by forming bonds with the equatorial atoms. Boron carbide can be considered as a binary alloy between boron and carbon, since it forms a single-phase solid solution over a relatively broad composition range, extending from ∼8 to ∼20 at.% C [1,11,12]. Due to the similarities of atomic form factors for x-ray diffraction [13] and nuclear scattering cross-sections (^{11}B and ^{12}C) for neutron diffraction [10,14] between boron and carbon atoms, experimentally distinguishing carbon from boron, and identifying their exact atomic positions, at any specific carbon content, are formidable tasks. First-principles calculations [15–23] predict two stable phases of boron carbide at 13.33 and 20 at.% C, corresponding to $B_{13}C_2$, and B_4C stoichiometries, respectively. The studies [15,17–22] suggest that, near the solubility limit (∼20 at.% C), the structural units of boron carbide are dominated by $B_{11}C^p$(C-B-C), where p stands for the polar sites, as shown by Fig. 1(a). Even though synthesis of boron carbide beyond the carbon-rich limit has been reported one time, ∼24 at.% C by Konovalikhin *et al.* [24], synthesizing boron carbide, where at.% C $\gtrsim$ 20, generally results in a mixture of boron carbide and free graphitelike carbon [11,25,26]. Recently, Jay *et al.* [27] suggested a possibility that the solubility range of boron carbide could be extended to 21.43 at.% C, in which, instead of the three-atom C-B-C chain, a structural model of $B_{11}C^p$(C-C), as shown in Fig. 1(b), was proposed and predicted, using first-principles calculations, to be metastable with respect to B_4C.

Although boron carbide has been intensively studied both experimentally and theoretically, there are still unresolved questions, debatable among the researchers, regarding the maximum at.% C [1,11,12,21,24,27,28], the extent of configurational disorder [22,23,29,30], the electronic band gap [15,22,31–35], and stability under high pressure [31,36–39], thus deserving further investigation. Recent theoretical studies of boron carbide [22,23,29,40] demonstrated that configurational disorder of boron and carbon atoms on the different lattice positions, activated at elevated temperatures, determines several properties. Moreover, a recent experimental study of $B_{4.3}C$ under high pressures up to ∼70 GPa [31] reveals a phase transition in $B_{4.3}C$ near 40 GPa, as indicated by the changes in the observed Raman spectra and the optical properties of $B_{4.3}C$. However, a detailed understanding regarding the structural change of $B_{4.3}C$ under high pressures has yet to be achieved. We note that high-pressure experimentation on boron carbide is often done in a diamond anvil cell [31,36,37], which highlights the importance of revealing the details of

*anekt@ifm.liu.se

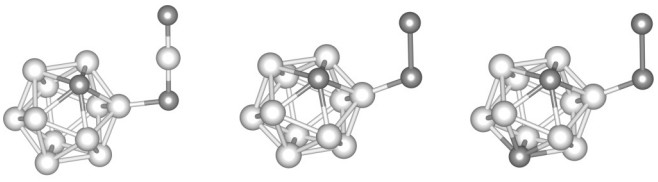

FIG. 1. Structural units of carbon-rich boron carbide at (a) 20 at.% C-$B_{11}C^p$(C-B-C), (b) 21.43 at.% C-$B_{11}C^p$(C-C), and (c) 28.57 at.% C-$B_{10}C_2^p$(C-C). White and gray spheres represent boron and carbon atoms, respectively.

high-pressure stabilities of boron carbide in a carbon-rich environment, as it could react with carbon at high pressure and temperature, and thus the interactions between boron carbide and carbon under such extreme conditions must be considered [41,42]. The carbon-rich side has also been studied in the form of turbostratic graphitelike phases, generally denoted by t-BC_x, where $x \geqslant 1$. When subjected to high pressure and high temperature, a direct transformation of t-BC_x into superhard diamondlike phases (c-BC_x) [43–46] as well as a phase decomposition of t-BC_x into icosahedral boron carbides and boron-doped diamond [43,47] have been reported in the literature.

In the present work, we investigate the stability of carbon-rich boron carbides, ranging from 20 to 33.33 at.% C, as a function of temperature and pressure, using first-principles calculations. We find that, apart from B_4C, carbon-rich boron carbide with 28.57 at.% C, denoted by $B_{2.5}C$, is thermodynamically stable under high pressures with respect to B_4C and its constituent elements, i.e., γ-boron and diamond. $B_{2.5}C$ is an electrical semiconductor, whose structural unit is represented by $B_{10}C_2^p$(C-C), in which the icosahedral C^p atoms arrange themselves in a way that the formation of both an inter- and intra-icosahedral C-C bond is avoided, as shown in Fig. 1(c). By inspecting its phonon frequencies and elastic constants, we find that $B_{2.5}C$ is both dynamically and mechanically stable at 0 GPa. To determine the thermodynamic stability of B_4C and $B_{2.5}C$, we calculate the Gibbs free energy, in which the contributions from the lattice vibration and the configurational disorder are obtained within the quasiharmonic and the mean-field approximations, respectively. The stabilities of B_4C and $B_{2.5}C$ are then illustrated through the p-T phase diagrams.

II. METHODOLOGY

A. Computational details

The density functional theory (DFT) and the projector augmented wave (PAW) method [48], as implemented in the Vienna *ab initio* simulation package (VASP) [49,50], and the generalized gradient approximation (GGA), proposed by Perdew, Burke, and Ernzerhof (PBE96) for an exchange-correlation functional [51], are used for the total energy calculations. The calculations are performed within a unit cell and a 2×2×2 supercell (64–224 atoms, depending on composition), sampled with a 9×9×9 and a 7×7×7 Monkhorst-Pack **k**-point mesh [52], respectively. A plane-wave energy cutoff of 600 eV is used. The equilibrium volume at 0 K, V_0, is determined by the minimum point of the total energy curve, $E_0(V)$, calculated for a set of different fixed volumes V. For each volume, the internal atomic positions and the cell shape are fully relaxed so that the total force, acting on each atom, is less than 10^{-6} eV/Å. The tetrahedron method for the Brillouin zone integrations, suggested by Blöchl [53], is used for electronic density-of-states calculations.

B. Thermodynamic stability

The thermodynamic stability of the carbon-rich boron carbides, especially B_4C and $B_{2.5}C$, with respect to their competing phases at different pressures p and temperatures T, is determined by the Gibbs free energy $G(T, p)$,

$$G(T,p) = E_0(V) + F_{\text{vib}}(T,V) - TS_{\text{conf}}(T,V) + pV. \quad (1)$$

$E_0(V)$ is the total energy at 0 K, directly obtained from the DFT calculations. $F_{\text{vib}}(T, V)$ is the Helmholtz free energy due to the lattice vibrations (phonons), which is generally given by

$$F_{\text{vib}}(T,V) = \frac{1}{2}\sum_{\mathbf{q},\nu}\hbar\omega(\mathbf{q},\nu,V) + k_BT\sum_{\mathbf{q},\nu}\ln\{1-\exp \times[-\hbar\omega(\mathbf{q},\nu,V)/k_BT]\}, \quad (2)$$

where $\omega(\mathbf{q},\nu,V)$ is the phonon frequency at the wave vector $\mathbf{q}$ and the band index ν. $\hbar$ and k_B are the reduced Planck constant and the Boltzmann constant, respectively. In this work, the phonon frequencies ω are also volume-dependent, as the phonon calculations are performed at the quasiharmonic level using the PHONOPY package for phonon calculations [54,55], in which the force constants are calculated within a 2×2×2 supercell using the Parlinski-Li-Kawazoe method [56] with a finite displacement of 0.01 Å.

The term $TS_{\text{conf}}(T, V)$ in Eq. (1) is a contribution from the configurational disorder, where S_{conf} is defined as the configurational entropy. In the present work, S_{conf} is derived within the mean-field approximation and is volume- and temperature-independent,

$$S_{\text{conf}} = k_B\ln(g), \quad (3)$$

where g is the number of distinguishable ways of arranging the atoms on the lattice sites. In the case of boron carbide, configurational disorder of icosahedral C^p atoms at the polar sites [22,29], for example, contributes S_{conf}, while it is generally zero for ordered compounds.

To determine the term pV and include it in $G(T, p)$ at fixed temperatures, the sums of the first three terms on the right-hand side of Eq. (1) at different fixed volumes are fitted to the third-order Birch-Murnaghan equation of state (EOS) [57,58]. The pressure p can then be calculated by

$$p = -\left[\frac{\partial[E_0(V) + F_{\text{vib}}(T,V) - TS_{\text{conf}}]}{\partial V}\right]_T. \quad (4)$$

We note that, in the present work, the contribution from electronic excitations to the Gibbs free energy $G(T, p)$ at high temperature is neglected due to the semiconducting character of the relevant phases, and it will be discussed in detail in Sec. III D.

C. Elastic properties calculations

The elastic properties of $B_{2.5}C$, are calculated at zero temperature ($T = 0$ K) and zero pressure ($p = 0$ GPa) conditions. We also neglect the influence of the zero-point motion. Consequently, the Gibbs free energy G, given in Eq. (1), reduces to the total electronic energy E_0. By applying strains ϵ with $\pm 1\%$ and $\pm 2\%$ distortions to the fully relaxed $2\times2\times2$ supercells without volume conservation, the elastic constants C_{ij} can be calculated directly from the second-order Taylor expansion of the total energy E_0 [59,60],

$$C_{ij} = \frac{1}{V_0}\frac{\partial^2 E_0(\epsilon_1,\ldots,\epsilon_6)}{\partial\epsilon_i\partial\epsilon_j}\bigg|_0. \tag{5}$$

We use Voigt's notation to describe the strain ϵ_i and the elastic tensor C_{ij} [61,62]. $E_0(\epsilon_1,\ldots,\epsilon_6)$ is the total energy of the supercell, distorted by the correspondingly applied strains ϵ_i. V_0 is the equilibrium volume of the undistorted supercell. Since the substitution of carbon atoms for boron atoms, residing in the icosahedra, breaks the $R\bar{3}m$ symmetry by a small distortion, as generally displayed in B_4C [17,21,22], we employ the projection technique, suggested by Moakher *et al.* [63], to derive the rhombohedrally averaged elastic constants $\bar{C}_{ij}$, following the procedure described in our previous work [40] for boron carbide and boron suboxide. In this case, 12 independent elastic constants, i.e., C_{11}, C_{12}, C_{13}, C_{14}, C_{22}, C_{23}, C_{24}, C_{33}, C_{44}, C_{55}, C_{56}, and C_{66}, must be calculated to obtain the six averaged elastic constants for $B_{2.5}C$, given by

$$\bar{C}_{11} = \tfrac{3}{8}(C_{11}+C_{22}) + \tfrac{1}{4}C_{12} + \tfrac{1}{2}C_{66}, \tag{6a}$$
$$\bar{C}_{12} = \tfrac{1}{8}(C_{11}+C_{22}) + \tfrac{3}{4}C_{12} - \tfrac{1}{2}C_{66}, \tag{6b}$$
$$\bar{C}_{13} = \tfrac{1}{2}(C_{13}+C_{23}), \tag{6c}$$
$$\bar{C}_{14} = \tfrac{1}{4}C_{14} - \tfrac{1}{4}C_{24} + \tfrac{1}{2}C_{56}, \tag{6d}$$
$$\bar{C}_{33} = C_{33}, \tag{6e}$$
$$\bar{C}_{44} = \tfrac{1}{2}C_{44} + C_{55}, \tag{6f}$$
$$\bar{C}_{66} = \tfrac{1}{2}(\bar{C}_{11} - \bar{C}_{12}). \tag{6g}$$

The elastic stability of $B_{2.5}C$ is inspected using the Born stability criteria [64], given by

$$\bar{C}_{11} - |\bar{C}_{12}| > 0, \tag{7a}$$
$$(\bar{C}_{11} + \bar{C}_{12})\bar{C}_{33} - 2(\bar{C}_{13})^2 > 0, \tag{7b}$$
$$(\bar{C}_{11} - \bar{C}_{12})\bar{C}_{44} - 2(\bar{C}_{14})^2 > 0, \tag{7c}$$
$$\bar{C}_{44} > 0. \tag{7d}$$

We use the Voigt-Reuss-Hill (VRH) method for determining the elastic properties of polycrystalline solids [65] to determine the isotropic elastic Young's, shear, and bulk moduli of $B_{2.5}C$.

III. RESULTS AND DISCUSSION

A. Thermodynamic stability at $T = 0$ K

As a first step, we determine the thermodynamic stability at $T = 0$ K, and $p = 0$ GPa of carbon-rich boron carbides with five different carbon contents, ranging from 20 to 33.33 at.% C. We note that, at this stage, the influence of lattice dynamics, i.e., the zero-point motion, is being neglected. Thus the Gibbs free energy G, given in Eq. (1), is defined only by the ground-state energy $E_0(V_0)$, and the stability of carbon-rich boron carbides with respect to their competing phases is determined by the formation energy ΔE_0^{form}. In the case of 26.67, 28.57, and 33.33 at.% C, where at least two C^p atoms are residing in the icosahedra, a formation of both intra- and inter-icosahedral bonds between C^p atoms is possible. By performing spin-polarized calculations, $B_{11}C^p$(C-C-C) and $B_{10}C_2^p$(C-C-C) with the intra-icosahedral C^p-C^p favor a magnetic state with a magnetic moment of $1\mu_B$ and $2\mu_B$, respectively. As can be seen from Table I, boron carbides with at.% C = 20, 21.43, and 28.57, corresponding to designations (configurations) of B_4C [$B_{11}C^p$(C-B-C)], $B_{3.67}C$ [$B_{11}C^p$(C-C)], and $B_{2.5}C$ [$B_{10}C_2^p$(C-C)], respectively, are stable with respect to their constituent elements, given by α-boron and diamond, while the others with at.% C = 26.67 and 33.33 are not stable, as indicated by considerably higher ΔE_0^{form}. We note that, in the present work, diamond has been considered as a competing phase of carbon at low pressure instead of graphite due to

TABLE I. Formation energy (ΔE_0^{form}) of different carbon-rich boron carbides (at.% C $\geqslant$ 20) in meV/atom with respect to (i) α-boron + diamond, and (ii) B_4C + diamond.

Stoichiometry	Configuration	at.% C	Type of C^p-C^p bond	$\Delta E^{\text{form}}_{\alpha\text{-boron+diamond}}$	$\Delta E^{\text{form}}_{B_4C+\text{diamond}}$
B_4C [Fig. 1(a)]	$B_{11}C^p$(C-B-C)	20.00	No	–128 (−148[a])	0
$B_{3.67}C$ [Fig. 1(b)]	$B_{11}C^p$(C-C)	21.43	No	–23 (−40[a])	103
$B_{2.75}C$	$B_{11}C^p$(C-C-C)	26.67	No	41	158
$B_{2.75}C$	$B_{10}C_2^p$(C-B-C)	26.67	No	62	179
$B_{2.75}C$	$B_{10}C_2^p$(C-B-C)	26.67	Intra-icosahedral	37	155
$B_{2.75}C$	$B_{10}C_2^p$(C-B-C)	26.67	Inter-icosahedral	109	227
$B_{2.5}C$ [Fig. 1(c)]	$B_{10}C_2^p$(C-C)	28.57	No	−72	43
$B_{2.5}C$	$B_{10}C_2^p$(C-C)	28.57	Intra-icosahedral	−47	67
$B_{2.5}C$	$B_{10}C_2^p$(C-C)	28.57	Inter-icosahedral	–7.4	107
B_2C	$B_{10}C_2^p$(C-C-C)	33.33	No	181	288
B_2C	$B_{10}C_2^p$(C-C-C)	33.33	Intra-icosahedral	214	320
B_2C	$B_{10}C_2^p$(C-C-C)	33.33	Inter-icosahedral	253	360

[a]Reference [27] [Jay *et al.* (GGA-PW91)].

the van der Waals interactions between the carbon layers that cannot be accurately accounted by standard DFT calculations, and thus rather sophisticated and time consuming approaches, e.g., van der Waals density functional (vdW-DF), are required to solve the issue [66–69]. As demonstrated by Shin *et al.* [70], the energy difference between graphite and diamond is somehow particularly small. Thus considering diamond as the competing phase instead of graphite would not qualitatively affect the stabilities of carbon-rich boron carbides. We note further that our calculations of ΔE_0^{form} for B_4C and $B_{3.67}C$ are in fairly good agreement with the previous calculations that used a different type of GGA functional [27]. We find that, for $B_{2.5}C$, the formation of the intra- and inter-icosahedral C^p-C^p bond results in higher ΔE_0^{form} than those without the C^p-C^p bond by at least ∼25 meV/atom. This indicates that the intra- and inter-icosahedral C^p-C^p bonds are an unfavorable type of bonding for $B_{2.5}C$, which is in line with the conclusion of our previous study of B_4C [22]. The stability of carbon-rich boron carbides is also examined with respect to B_4C and diamond, since B_4C has been predicted to be a stable phase for boron carbide [15,17–22], and presumably lies on the convex hull of the B-C system [21]. The results demonstrate that none of the carbon-rich boron carbides is stable with respect to B_4C and diamond at $T = 0$ K and $p = 0$ GPa.

Based on the results mentioned above, we single out those, stable with respect to α-boron and diamond, and investigate the influence of high pressures on their stabilities, determined by the formation enthalpy ΔH^{form}. The enthalpy $H(p)$ at 0 K can be calculated by

$$H(p) = E_0(V) + pV. \tag{8}$$

We find that $B_{2.5}C$ without the C^p-C^p bond lies on the convex hull above 40 GPa, as shown in Fig. 2, and is stable up to 57 GPa with respect to both B_4C and its constituent elements, given by γ-boron, which is a high-pressure phase of boron,

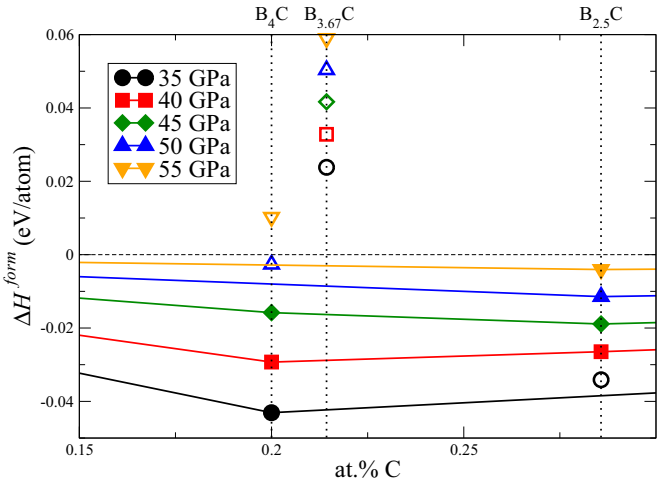

FIG. 2. Formation enthalpy ΔH^{form} with respect to γ-boron and diamond of B_4C, $B_{3.67}C$, and $B_{2.5}C$ without the inter- and intra-icosahedral C^p-C^p bond under pressures, ranging from 35 to 55 GPa. Filled and open symbols indicate the carbon-rich boron carbides, which are lying on and above the convex hulls at different fixed pressures, respectively.

and diamond. Note that, in the present work, γ-boron is predicted to be stable over α-boron above 18.8 GPa, which is in good agreement with the value reported in the literature [71,72], while the conversion of graphite to diamond at low temperature, according to the proposed phase diagram of carbon [73–75], has been expected to take place at $p < 5$ GPa. As for the other two $B_{2.5}C$ candidate phases, where there exist the inter- and intra-icosahedral C^p-C^p bonds, we find that upon increasing the applied pressure they become unstable with respect to the constituent elements above 15 and 37 GPa, respectively. B_4C, on the other hand, becomes unstable with respect to $B_{2.5}C$ without the C^p-C^p bond and γ-boron at $p >$ 47 GPa.

In the case of $B_{3.67}C$, despite being stable with respect to α-boron and diamond at 0 GPa, it does not touch the convex hull upon increasing the applied pressure. We find that, at $p >$ 25 GPa, $B_{3.67}C$ becomes unstable with respect to γ-boron and diamond, which is indicated by positive ΔH^{form}, as shown in Fig. 2. We thus disprove the stability of $B_{3.67}C$ or $B_{11}C^p$(C-C), recently proposed in Ref. [27]. Based on these findings, only B_4C and $B_{2.5}C$ without the C^p-C^p bond, which from now on will be referred to as just $B_{2.5}C$, will be further investigated in the following sections.

B. Configurational disorder in $B_{2.5}C$

We have learned from our previous studies [22,23,40] that configurational disorder plays an important role in the stability as well as the properties of boron carbides at elevated temperature. In the case of B_4C, configurational disorder of icosahedral C^p atoms either at the three polar sites, forming the top or bottom triangular face, or at all six polar sites of the icosahedra is predicted [22,29]. It is found to restore the higher rhombohedral symmetry in B_4C by eliminating a small monoclinic distortion, caused by the preferred orientation of the C^p atoms residing in the same polar site for every icosahedron, at low temperature in the ordered ground state of B_4C. Correspondingly, the ordered ground-state configuration of $B_{2.5}C$ is attained when the C^p atoms occupy the same polar positions for every icosahedron without forming either an inter- and intra-icosahedral bond between the C^p atoms. In this section, we investigate the influences of configurational disorder of icosahedral C^p atoms at the polar sites on the stability of $B_{2.5}C$. Configurational disorder in $B_{2.5}C$ is modeled within a $2\times2\times2$ supercell, where a random number generator is employed to randomly distributed the icosahedral C^p atoms among the polar sites. To avoid the C^p-C^p bonds, we assign two constraints that (i) only one C atom is allowed to reside in each triangular face, formed by the three polar sites, of the icosahedra, and (ii) any polar site that bonds to a C^p atom from a neighboring icosahedron must only be occupied by a B atom.

Based on the assumption we used for modeling the disordered $B_{2.5}C$, there are on average four distinguishable configurations that the two C^p atoms can arrange within each icosahedron. We thus estimate the configurational entropy S_{conf}/unit cell for the disordered $B_{2.5}C$, using Eq. (3), to be $k_B \ln(4)$, while $S_{\text{conf}} = 0$ for the ordered $B_{2.5}C$. We consider 10 different configurations of the disordered $B_{2.5}C$. The order-disorder transition temperature at 0 GPa can be calculated from

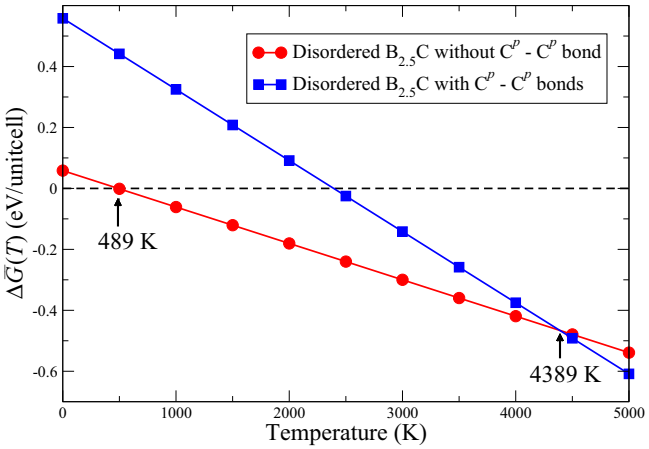

FIG. 3. Difference in Gibbs free energy $\Delta\bar{G}(T)$ at $p = 0$ GPa for disordered $B_{2.5}C$, relative to the ordered $B_{2.5}C$, and plotted as a function of temperature. Black arrows indicate the mean values of the transition temperatures.

the difference in the Gibbs free energy $\Delta G(T)$ with respect to the ordered phase, where the Gibbs free energy $G(T)$ is given by

$$G(T,0) = E_0(V_0) - T S_{\text{conf}}. \quad (9)$$

We note that due to the use of a random number generator, each model of the disordered $B_{2.5}C$ has different configuration of the C^p atoms from the others, giving rise to the uncertainties in $G(T)$ for the disordered $B_{2.5}C$ as well as the order-disorder transition temperature. To estimate such uncertainties, we calculate the mean values of both the Gibbs free energy, denoted by $\bar{G}(T)$, and the order-disorder transition temperature, and their standard deviations. The order-disorder transition temperature for $B_{2.5}C$ is thus 489 ± 54 K with 95% confidence intervals, as shown in Fig. 3.

To illustrate how the C^p-C^p bonds affect the stability of $B_{2.5}C$, we build up another 10 configurations of the disordered $B_{2.5}C$ by removing the two constraints so that the two C^p atoms residing in each icosahedron are allowed to substitute any two out of the six polar sites, and they thus have a possibility to form either the inter- or intra-icosahedral C^p-C^p bond with the other C^p atoms. By manually taking away the C^p-C^p bonds and recalculating their total energies, $E_0(V_0)$, we estimate the energy costs to form the intra- and inter-icosahedral C^p-C^p bonds from the changes in $E_0(V_0)$ to be $\sim$0.4 and $\sim$1.1 eV/bond, respectively. The S_{conf}/unit cell, in this case, is approximated to be $k_B \ln(15)$, and the transition to the disordered state with the C^p-C^p bonds is predicted to take place at 4389 ± 636 K (see Fig. 3), which is beyond the melting point of boron carbide ($\sim$2650 K [76]). These results thus indicate a strong correlation among the C^p atoms that tend to avoid the formation of the unfavorable C^p-C^p bond. Consequently, we conclude that the relevant configuration of $B_{2.5}C$ at elevated temperature can be described by configurational disorder of the icosahedral C atoms at the polar sites, where they arrange themselves in such a way that the formation of a C^p-C^p bond is avoided.

TABLE II. Lattice parameters and angles between them of $B_{2.5}C$, calculated in the present work, and B_4C, taken from Refs. [22] and [10].

	Lattice parameters a, b, c (Å/unit cell)	Angles α, β, γ (deg)
$B_{2.5}C$		
Order (Calc.)	4.849 4.939 4.849	68.20 68.56 68.20
Disorder (Calc.)	4.872 4.882 4.881	68.30 68.36 68.37
B_4C		
Order (Calc.)[a]	5.209, 5.209, 5.059	66.01, 66.01, 65.14
Disorder (Calc.)[b]	5.161, 5.161, 5.161	65.73, 65.73, 65.73
Expt.[b]	5.163, 5.163, 5.163	65.73, 65.73, 65.73

[a]Reference [22] [Ektarawong *et al.* (GGA-PBE96)].
[b]Reference [10] [Morosin *et al.* (Neutron diffraction)].

C. Structural, electronic, and elastic properties of $B_{2.5}C$

In this subsection, the structural, electronic, and elastic properties of $B_{2.5}C$ are reported. Table II shows the lattice parameters of $B_{2.5}C$ and B_4C [10,22] with and without configurational disorder of the icosahedral C atoms at the polar sites. As mentioned in the previous subsection, substitution of C atoms in the icosahedra in general results in a small distortion that breaks the rhombohedral symmetry ($R\bar{3}m$) of boron carbide. This is often illustrated through the ordered B_4C [17,21,22], where the icosahedral C atoms are well oriented by occupying the same polar position for every icosahedron. However, recent theoretical studies [22,29] demonstrated that configurational disorder in the disordered B_4C, in which the icosahedral C atoms are randomly distributed at the polar sites, eliminates the distortion, and thus restores the rhombohedral symmetry, which is in accord with the experimentally observed crystal symmetry of boron carbide [7–10]. Similarly to the ordered B_4C, the ordered $B_{2.5}C$ exhibits the same distortion. Even though the rhombohedral symmetry is not completely restored for the disordered $B_{2.5}C$ (see Table II), the degree of distortion becomes obviously smaller, compared to that of the ordered phase. The lack of complete restoration of the rhombohedral symmetry is attributed to an uneven distribution of the icosahedral C atoms at the six polar sites within a finite-size supercell when modeling the disordered $B_{2.5}C$. Thus, for an infinitely large supercell, the disordered $B_{2.5}C$ should exhibit rhombohedral symmetry with $R\bar{3}m$ space group, similar to the disordered B_4C.

According to the electron counting rules, proposed by Longuet-Higgins and Roberts [79], to interpret the electronic structure and stability of icosahedral boron-rich clusters, we find that $B_{2.5}C$ is an electron precise compound, whose valence band is completely filled up by the electrons, and thus it should display a semiconducting character. To verify this presumption, we calculate the electronic density of states of $B_{2.5}C$ at $p = 0$ GPa and $T = 0$ K, as shown in Fig. 4. The ordered and disordered $B_{2.5}C$ are both semiconductors with GGA-based electronic band gaps of 2.85 and 2.57 eV, respectively. The decrease in the gap width of the disordered $B_{2.5}C$ by $\sim$0.3 eV, compared to the ordered $B_{2.5}C$, can be explained by the random substitution of icosahedral C atoms at the polar sites, as we demonstrated also for B_4C in our previous work [22]. In the case of B_4C, the GGA-based band

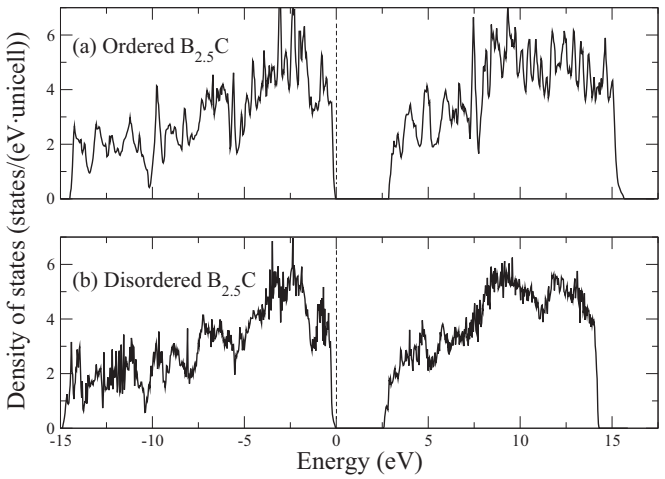

FIG. 4. Electronic density of states of (a) ordered $B_{2.5}C$ and (b) disordered $B_{2.5}C$, obtained by using GGA-PBE96 for the exchange-correlation functional. The dashed lines at 0 eV indicate the highest energy states occupied by the electrons.

gap of B_4C can vary between 2 and 3 eV depending on the degree of configurational disorder of the C^p atoms.

Next, we calculate the elastic properties of $B_{2.5}C$ at $p = 0$ GPa and $T = 0$ K, using the procedure described in Sec. II C. The calculated elastic constants and elastic moduli of $B_{2.5}C$ are listed in Table III. By evaluating the elastic stability of $B_{2.5}C$ using the Born stability criteria, given in Eq. (7), we find that all the criteria are fulfilled for both ordered and disordered $B_{2.5}C$, thus they are mechanically stable. Similarly to B_4C, configurational disorder of the C^p atoms has minimal impact on the elastic properties of $B_{2.5}C$, as indicated by almost identical elastic constants between the ordered and disordered $B_{2.5}C$. This is in contrast to the case of $B_{13}C_2$, where configurational disorder significantly affects its elastic properties [40]. We can also see from the table that $B_{2.5}C$ is distinctly superior to B_4C in terms of elastic moduli. For example, Young's modulus of $B_{2.5}C$ is higher than that of B_4C by ∼30%.

Demonstrated by several experimental and theoretical studies [1,11,80–82], boron carbides can be superhard materials, with Vickers hardness exceeding 40 GPa. Considering that $B_{2.5}C$ has even higher values of elastic moduli than those of B_4C, together with the experimental fact that hardness of boron carbide increases with the carbon content [83,84], one can expect the carbon-rich $B_{2.5}C$ to be a superhard material, likely even harder than B_4C.

D. Influences of lattice dynamics and thermodynamic stability at $T > 0$ K

We next investigate the influences of lattice vibrations on the stabilities of B_4C and $B_{2.5}C$. The vibrational free energies $F_{\rm vib}(T, V)$ of $B_{2.5}C$, B_4C, and their competing phases, i.e., α- and γ-boron, and diamond, are calculated within the quasiharmonic approximation, using the approaches described in Sec. II B. In the present work, the B-C compounds at the carbon-rich side, e.g., $BC_{1.6}$, BC_3, and BC_5, are not considered as competing phases of B_4C and $B_{2.5}C$ for the following reasons. At low pressure, those carbon-rich compounds exhibit turbostratic graphitelike phases, t-BC_x where $x \geqslant 1$. As demonstrated by Solozhenko *et al.* [43,47], t-BC_x, where $1 \leqslant x \leqslant 4$, decomposes into a mixture of boron-doped diamond (1–2 at.% B) and icosahedral boron carbides at $p > 20$ GPa and $T > 2000$ K. Additionally, even though a direct transformation of t-BC_x into superhard diamondlike phases (c-BC_x) under high pressure and temperature has been reported in the literature [43–46], they are shown to be metastable phases and unlikely to participate in the phase equilibria in the boron-carbon system [43,46]. We have thus expected that considering t-BC_x and c-BC_x as competing phases should not qualitatively and significantly affect our predictions of the stability ranges of B_4C and $B_{2.5}C$.

By considering the phonon density of states of the ordered and disordered phases of both $B_{2.5}C$ and B_4C, as shown in Fig. 5, their phonon frequencies are all positive, confirming their dynamical stabilities. We note that $B_{2.5}C$ and B_4C remain dynamically stable under high pressures, up to at least 75 GPa, as indicated by real phonon frequencies also at such pressures (not shown).

By comparing the vibrational free energies between the ordered and disordered phases of $B_{2.5}C$ and B_4C, we find

TABLE III. Averaged elastic constants $\bar{C}_{ij}$ (GPa), bulk modulus B_H (GPa), shear modulus G_H (GPa), Young's modulus E_H (GPa), Poisson's ratio ν_H, and B_H/G_H ratio in the Voigt-Reuss-Hill (VRH) approach for $B_{2.5}C$. Comparison is made with those of B_4C.

	$\bar{C}_{11}$	$\bar{C}_{12}$	$\bar{C}_{13}$	$\bar{C}_{14}$	$\bar{C}_{33}$	$\bar{C}_{44}$	B_H	G_H	E_H	ν_H	B_H/G_H	Ref.
$B_{2.5}C$												
Order (Calc.)	620	90	75	–23	605	290	258	275	609	0.10	0.94	This work
Disorder (Calc.)	621	90	74	–22	602	289	258	275	608	0.10	0.94	This work
B_4C												
Expt.							247	200	472	0.18	1.24	[77][a]
							235	197	462	0.17	1.19	[78][b]
Order (Calc.)	559	123	68	24	524	169	239	200	469	0.17	1.20	[40][c]
							233	202	470		1.15	[27][d]
Disorder (Calc.)	558	122	67	25	521	163	238	197	463	0.18	1.20	[40][c]

[a]Reference [77] [Gieske *et al.* (Expt.)].
[b]Reference [78] [Manghnani *et al.* (Expt.)].
[c]Reference [40] [Ektarawong *et al.* (GGA-PBE96)].
[d]Reference [27] [Jay *et al.* (GGA-PW91)].

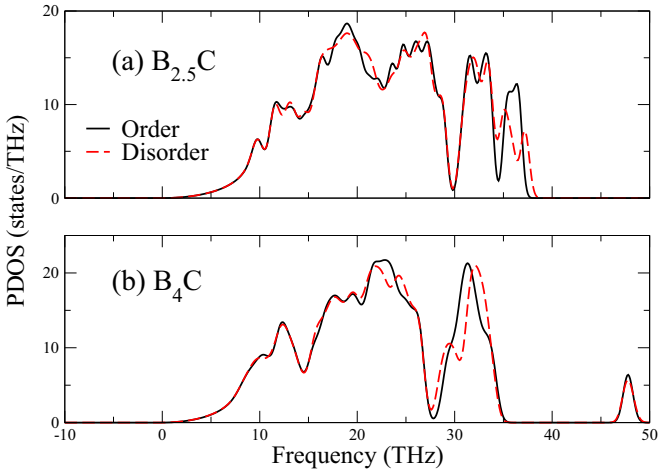

FIG. 5. Phonon density of states of (a) $B_{2.5}C$ and (b) B_4C at 0 GPa. The black solid and the red dashed lines indicate the phonon frequencies for the ordered and the disordered phases, respectively.

that configurational disorders have tiny impacts on their vibrational contributions to the Gibbs free energy, where the differences in the vibrational free energies between the ordered and disordered phases of $B_{2.5}C$ and B_4C are ~0.1 and ~0.8 meV/atom, respectively, at 2500 K. This is due to small changes in the equilibrium volumes of $B_{2.5}C$ and B_4C, i.e., $\sim 1.5\times10^{-3}$ and $\sim 6\times10^{-3}$ Å^3/atom, respectively, induced by configurational disorders.

According to our previous study of configurational disorder in B_4C [22], two configurational phase transitions at 0 GPa were predicted within the mean-field approximation for the configurational entropy S_{conf} at 870 and 2325 K, in which the icosahedral C atoms configurationally disorder only at the three polar sites, forming the top or bottom triangular face, and at all six polar sites of the icosahedra, respectively. In this case, the configurational entropies S_{conf}/unit cell for the first and the second disorder states of B_4C are estimated to be $k_B\ln(3)$ and $k_B\ln(6)$, respectively. We find that the influence of lattice vibrations, considered in the present work, lowers the order-disorder transition temperature of B_4C from 870 to 730 K.

We then determine the thermodynamics stabilities of $B_{2.5}C$ and B_4C with respect to their competing phases at different fixed pressures p and temperatures T by calculating the Gibbs free energy $G(T, p)$, given by Eq. (1). As mentioned in Sec. II B, the contributions from the electronic excitations is neglected in the present work. We note that $B_{2.5}C$, B_4C, and their competing phases, i.e., diamond, α-, and γ-boron, are predicted to be a semiconductor with the GGA-based electronic band gaps ranging between 1.5 and 3 eV, where the highest energy states occupied by the electrons, i.e., Fermi level, are located at the top edge of the valence band. At $T > 0$ K, a small fraction of the electrons within the range of thermal energy $\pm k_BT$ from the Fermi level can be thermally excited and contributes to the electronic part of the Gibbs free energy $G(T, p)$, assuming that at $T = 5000$ K, which is beyond the melting point of the considered materials, the thermal energy k_BT is only about 0.43 eV. Since there is no available state for the electrons to populate within such a range of k_BT above the valence-band edge of $B_{2.5}C$ and B_4C and their competing phases, regardless of the temperature dependence of the band gap, the contributions from the electronic excitations are approximated and expected to be essentially small even at very high temperature, and they are thus negligible. In the present work, we show the p-T phase diagrams for the two global compositions, i.e., $B_{2.5}C$ and B_4C, in Fig. 6.

We first consider the phase diagram of boron carbide at the $B_{2.5}C$ composition, as depicted in Fig. 6(a). We predict that under high pressures, ranging between 40 and 67 GPa depending on the temperatures, $B_{2.5}C$ is a thermodynamically stable phase, with respect to B_4C, γ-boron, and diamond. At $T \gtrsim 500$ K, the icosahedral C atoms in $B_{2.5}C$ configurationally disorder at the polar sites, as discussed in Sec. III B. Below 40 GPa, $B_{2.5}C$ is unstable and decomposes into B_4C and diamond, which is in line with the experimental observations that synthesizing boron carbide with at.% C $\gtrsim$ 20 generally results in a mixture of boron carbide and free carbon [11,25,26]. The stability range of $B_{2.5}C$ under very high pressures is limited, as it decomposes into γ-boron and diamond, for example at $p = 60$ GPa and $T = 1000$ K.

Figure 6(b), on the other hand, displays the stability of the B_4C composition of boron carbide. At $p \lesssim 47$ GPa, B_4C is predicted to be stable with respect to $B_{2.5}C$ and its constituent elements. We find that as the pressure increases, the order-disorder transition temperature of B_4C increases. Beyond ~47 GPa, B_4C becomes unstable and decomposes into γ-boron and $B_{2.5}C$, stable within a limited stability range, before it subsequently decomposes into γ-boron and diamond upon increasing pressure.

Note that apart from our previous study of configurational disorder in B_4C [22], the same configurational phase transitions in B_4C were also predicted by Yao *et al.* [29]. However, in their case, the second configurational phase transition was predicted to take place at much lower temperature, i.e., 790 K. Thus, to assess a lower limit for the stability of $B_{2.5}C$, we estimate the configurational entropy S_{conf} for the disordered state of B_4C to be $k_B\ln(6)$ instead of $k_B\ln(3)$. The conservative estimate of the stability of $B_{2.5}C$ under high pressures is indicated by the dashed lines, as shown in Fig. 6. Despite narrowing the stability range, $B_{2.5}C$ is still stable at high pressures and also at high temperatures. We thus propose a carbon-rich icosahedral boron carbide $B_{2.5}C$, beyond 20 at.% C, to be stable under high pressures, and possibly metastable at ambient pressure.

E. Synthesis route of $B_{2.5}C$ and fingerprint for its characterization

According to the sketched phase diagrams, as shown in Fig. 6, $B_{2.5}C$ can be thermodynamically stabilized under high pressures. To experimentally synthesize $B_{2.5}C$, one may try compressing boron carbide powder, with at.% C close to 20, within a diamond anvil cell to high pressures around 50 GPa. Together with boron carbide, graphite powder, acting as a carbon reservoir, may be added into the diamond cell to assist in the formation of carbon-rich $B_{2.5}C$. Note that the diamond cell itself is also a carbon reservoir, and thus in light of our finding, reaction of the diamond cell with boron carbide under high pressure and high temperature must be considered. During the high-pressure compression, annealing of the powders at elevated temperatures should be provided

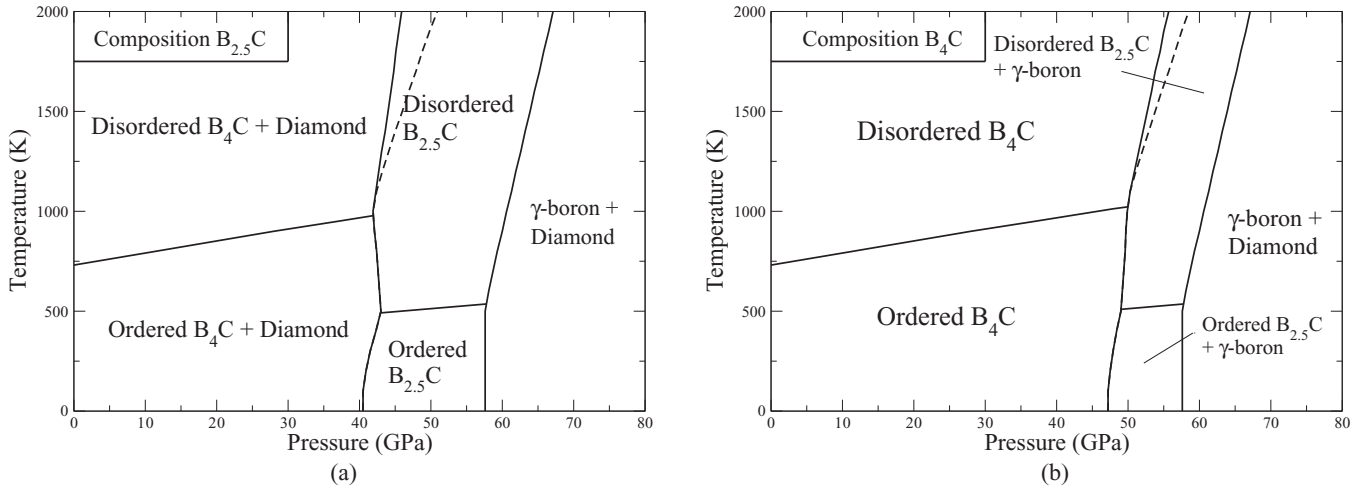

FIG. 6. *p-T* phase diagram of the composition: (a) $B_{2.5}C$ and (b) B_4C. The dashed lines indicate a conservative lower bound of the stability of $B_{2.5}C$, where the configurational entropy of B_4C is maximized to be $k_B\ln(6)$ (see main text for details).

in order to activate a solid-state reaction between boron carbide and a carbon reservoir, leading to a formation of $B_{2.5}C$. We note that, due to strong interatomic covalent bonds, which are typical characteristics of icosahedral boron-rich solids, high temperatures ranging between 1600 and 2000 K might be required in order to activate atomic diffusion in boron carbide [25,26,85]. After the heating process, the substance should be quenched to room temperature without depressurizing the diamond cell. Thus we suggest that a phase decomposition of $B_{2.5}C$ into B_4C and graphite after depressurizing the diamond cell, that would require long-range diffusion, could be hindered by a lack of atomic mobility at low temperatures.

The lattice parameters (angles) of $B_{2.5}C$, as shown in Table II, are significantly smaller (larger) than those of B_4C by approximately 5.4% (4%), corresponding to a decrease of unit-cell volume in $B_{2.5}C$ by 11.6%, as compared to that of B_4C. Such a volume contraction in $B_{2.5}C$ is mainly due to the formation of diatomic carbon chains, instead of three-atom chains, commonly formed for boron carbides with at.% $\lesssim 20$ [86]. For this reason, the existence of the carbon-richer phase $B_{2.5}C$ may be investigated by conventional diffraction techniques. Figure 7 shows a comparison between simulated powder diffraction patterns at zero pressure of disordered B_4C and $B_{2.5}C$. The simulated powder diffraction patterns, in the present work, are obtained from the RIETAN-FP package [87], as implemented in VESTA [88]. We find that the pattern of B_4C, obtained from the simulation, is in excellent agreement with the data taken from the International Centre for Diffraction Data (ICDD) card 00-035-0798 for B_4C, confirming the reliability of our simulations. As can be seen from Fig. 7, the diffraction pattern of $B_{2.5}C$, especially the main peaks within the range between 15° and 45° [Fig. 7(a)], is distinctly different from that of B_4C in terms of peak positions. It is thus feasible to use the diffraction patterns, given in Fig. 7, as a fingerprint to identify $B_{2.5}C$.

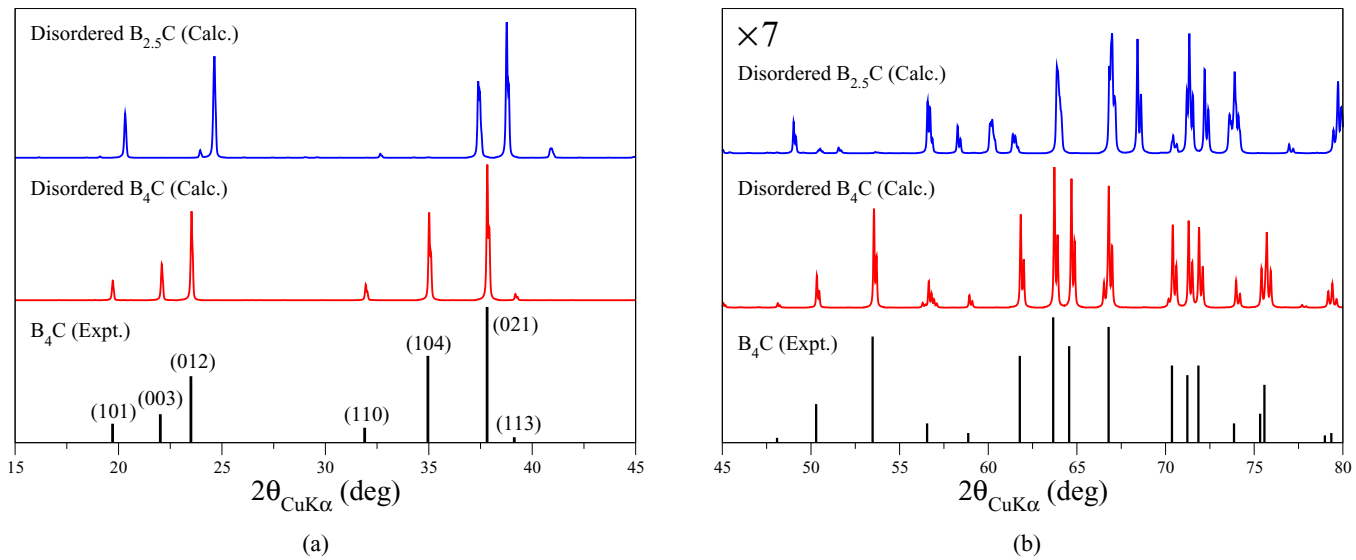

FIG. 7. Simulated x-ray powder diffraction patterns (Cu $K\alpha$) of disordered B_4C (red) and $B_{2.5}C$ (blue). The experimental powder diffraction of B_4C (black), taken from the International Centre for Diffraction Data (ICDD) card 00-035-0798, is given for comparison.

IV. CONCLUSION

In conclusion, we investigate, using first-principles calculations, the thermodynamic stabilities at finite temperature and pressure of different carbon-rich icosahedral boron carbides, ranging from 20 to 33.33 at.% C. We find that, apart from B_4C, extensively studied and addressed in the literature, only boron carbide at 28.57 at.% C, or $B_{2.5}C$, is predicted to be thermodynamically stable under high pressures with respect to B_4C, γ-boron, and diamond. The atomic configuration of the predicted $B_{2.5}C$ is represented by $B_{10}C_2^p$(C-C), in which the icosahedral C^p atoms residing in the polar sites of the icosahedra arrange themselves in a way that avoids the formation of either inter- or intra-icosahedral C^p-C^p bonds.

In the present work, the thermodynamic stability of $B_{2.5}C$ is illustrated through p-T phase diagrams at $B_{2.5}C$ and B_4C compositions, sketched at the quasiharmonic level for the contributions from the lattice dynamics, while the influence of configurational disorder is taken into account within the mean-field approximation for the configurational entropy. Depending on the temperature, the stability range of $B_{2.5}C$ is predicted to be within the range between 40 and 67 GPa. At $T \gtrsim 500$ K, the icosahedral C^p atoms in $B_{2.5}C$ configurationally disorder at the polar sites. By inspecting its phonon frequencies and elastic constants, $B_{2.5}C$ is shown to be both dynamically and mechanically stable also at 0 GPa.

Based on the phase diagrams, a possible high-pressure route for experimental synthesis of $B_{2.5}C$ has been suggested. Also, we emphasize that $B_{2.5}C$ should be taken into consideration in high-pressure experiments of B_4C, carried out in diamond anvil cells, as it could react with diamond under high pressure, possibly resulting in the formation of $B_{2.5}C$. The simulated powder diffraction pattern of $B_{2.5}C$ reveals a distinct difference in terms of peak positions with respect to that of B_4C, which may be used as a fingerprint to distinguish it from B_4C during attempts of experimental synthesis.

ACKNOWLEDGMENTS

Financial support by the Swedish Research Council (VR) through the Young Researcher Grant No. 621-2011- 4417 and the International Career Grant No. 330-2014-6336 and Marie Sklodowska Curie Actions, Cofund, Project INCA 600398 is gratefully acknowledged by B.A. The support from CeNano at Linköping University is acknowledged by A.E. and B.A. S.I.S. acknowledges the Swedish Research Council (VR) Project No. 2014-4750, LiLi-NFM. B.A. and S.I.S acknowledge support from the Swedish Government Strategic Research Area in Materials Science on Functional Materials at Linköping University (Faculty Grant SFO-Mat-LiU No. 2009 00971). The simulations were carried out using supercomputer resources provided by the Swedish National Infrastructure for Computing (SNIC) performed at the National Supercomputer Centre (NSC) and the Center for High Performance Computing (PDC).

[1] F. Thevénot, Boron carbide—A comprehensive review, J. Eur. Ceram. Soc. **6**, 205 (1990).
[2] D. Emin, Unusual properties of icosahedral boron-rich solids, J. Solid State Chem. **179**, 2791 (2006).
[3] D. Emin, Icosahedral boron-rich solids, Phys. Today **40**(1), 55 (1987).
[4] J. E. Zorzi, C. A. Perottoni, and J. A. H. da Jornada, Hardness and wear resistance of B_4C ceramics prepared with several additives, Mater. Lett. **59**, 2932 (2005).
[5] H. Werheit, Boron-rich solids: A chance for high-efficiency high-temperature thermoelectric energy conversion, Mater. Sci. Eng. B **29**, 228 (1995).
[6] T. L. Aselage, D. Emin, C. Wood, I. Mackinnon, and I. Howard, Anomalous Seebeck coefficient in boron carbides, MRS Proc. **97**, 27 (1987).
[7] H. K. Clark and J. L. Hoard, The crystal structure of boron carbide, J. Am. Chem. Soc. **65**, 2115 (1943).
[8] H. L. Yakel, The crystal structure of a boron-rich boron carbide, Acta Crystallogr. Sect. B **31**, 1797 (1975).
[9] B. Morosin, A. W. Mullendore, D. Emin, and G. A. Slack, in *Rhombohedral Crystal Structure of Compounds Containing Boron-rich Icosahedra*, AIP Conf. Proc. No. 140 (AIP, New York, 1986), p. 70.
[10] B. Morosin, G. H. Kwei, A. C. Lawson, T. L. Aselage, and D. Emin, Neutron powder diffraction refinement of boron carbides. Nature of intericosahedral chains, J. Alloys Compd. **226**, 121 (1995).
[11] V. Domnich, S. Reynaud, R. A. Haber, and M. Chhowalla, Boron carbide: Structure, properties, and stability under stress, J. Am. Ceram. Soc. **94**, 3605 (2011).
[12] H. Okamoto, B-C (boron-carbon), J. Phase Equilib. **13**, 436 (1992).
[13] I. Jiménez, D. G. Sutherland, T. van Buuren, J. A. Carlisle, L. J. Terminello, and F. J. Himpsel, Photoemission and x-ray absorption study of boron carbide and its surface thermal stability, Phys. Rev. B **57**, 13167 (1998).
[14] V. F. Sears, Neutron scattering lengths and cross sections, Neutron News **3**, 26 (1992).
[15] D. M. Bylander, L. Kleinman, and S. Lee, Self-consistent calculations of the energy bands and bonding properties of $B_{12}C_3$, Phys. Rev. B **42**, 1394 (1990).
[16] D. M. Bylander and L. Kleinman, Structure of $B_{13}C_2$, Phys. Rev. B **43**, 1487 (1991).
[17] R. Lazzari, N. Vast, J. M. Besson, S. Baroni, and A. D. Corso, Atomic Structure and Vibrational Properties of Icosahedral B_4C Boron Carbide, Phys. Rev. Lett. **83**, 3230 (1999).
[18] F. Mauri, N. Vast, and C. J. Pickard, Atomic Structure of Icosahedral B_4C Boron Carbide from a First Principles Analysis of NMR Spectra, Phys. Rev. Lett. **87**, 085506 (2001).
[19] J. E. Saal, S. Shang, and Z. K. Liu, The structural evolution of boron carbide via ab initio calculations, Appl. Phys. Lett. **91**, 231915 (2007).
[20] N. Vast, J. Sjakste, and E. Betranhandy, Boron carbides from first principles, J. Phys.: Conf. Ser. **176**, 012002 (2009).
[21] M. Widom and W. P. Huhn, Prediction of orientational phase transition in boron carbide, Solid State Sci. **14**, 1648 (2012).
[22] A. Ektarawong, S. I. Simak, L. Hultman, J. Birch, and B. Alling, First-principles study of configurational disorder in B_4C using a superatom-special quasirandom structure method, Phys. Rev. B **90**, 024204 (2014).

[23] A. Ektarawong, S. I. Simak, L. Hultman, J. Birch, and B. Alling, Configurational order-disorder induced metal-nonmetal transition in $B_{13}C_2$ studied with first-principles superatom-special quasirandom structure method, Phys. Rev. B **92**, 014202 (2015).

[24] S. V. Konovalikhin and V. I. Ponomarev, Carbon in boron carbide: The crystal structure of $B_{11.4}C_{3.6}$, Russ. J. Inorg. Chem. **54**, 197 (2009).

[25] C. Pallier, J.-M. Leyssale, L. A. Truflandier, A. T. Bui, P. Weisbecker, C. Gervais, H. E. Fischer, F. Sirotti, F. Teyssandier, and G. Chollon, Structure of an amorphous boron carbide film: An experimental and computational approach, Chem. Mater. **25**, 2618 (2013).

[26] J. K. Sonber, T. S. R. Ch. Murthy, C. Subramanian, R. K. Fotedar, R. C. Hubli, and A. K. Suri, Synthesis, densification and characterization of boron carbide, Trans. Ind. Ceram. Soc. **72**, 100 (2013).

[27] A. Jay, N. Vast, J. Sjakste, and O. H. Duparc, Carbon-rich icosahedral boron carbide designed from first principles, Appl. Phys. Lett. **105**, 031914 (2014).

[28] K. A. Schwetz and P. Karduck, in *Investigations in the Boron-carbon System with the Aid of Electron Probe Microanalysis*, AIP Conf. Proc. No. 231 (AIP, New York, 1991), p. 405.

[29] S. Yao, W. P. Huhn, and M. Widom, Phase transitions of boron carbide: Pair interaction model of high carbon limit, Solid State Sci. **47**, 21 (2015).

[30] S. Mondal, E. Bykova, S. Dey, S. I. Ali, N. Dubrovinskaia, L. Dubrovinsky, G. Parakhonskiy, and S. van Smaalen, Disorder and defects are not intrinsic to boron carbide, Sci. Rep. **6**, 19330 (2016).

[31] A. Hushur, M. H. Manghnani, H. Werheit, P. Dera, and Q. Williams, High-pressure phase transition makes $B_{4.3}C$ boron carbide a wide-gap semiconductor, J. Phys.: Condens. Matter **28**, 045403 (2016).

[32] K. Shirai, Electronic structures and mechanical properties of boron and boron-rich crystals (Part I), J. Superhard Mater. **32**, 205 (2010).

[33] V. I. Ivashchenko and V. I. Shevchenko, First-principles study of the atomic and electronic structures of crystalline and amorphous B_4C, Phys. Rev. B **80**, 235208 (2009).

[34] H. Dekura, K. Shirai, and A. Yanase, Metallicity of boron carbides at high pressure, J. Phys.: Conf. Ser. **215**, 012117 (2010).

[35] H. Werheit, On excitons and other gap states in boron carbide, J. Phys.: Condens. Matter **18**, 10655 (2006).

[36] T. Fujii, Y. Mori, H. Hyodo, and K. Kimura, X-ray diffraction study of B_4C under high pressure, J. Phys.: Conf. Ser. **215**, 012011 (2010).

[37] X. Q. Yan, Z. Tang, L. Zhang, J. J. Guo, C. Q. Jin, Y. Zhang, T. Goto, J. W. McCauley, and M. W. Chen, Depressurization Amorphization of Single-Crystal Boron Carbide, Phys. Rev. Lett. **102**, 075505 (2009).

[38] T. J. Vogler, W. D. Reinhart, and L. C. Chhabildas, Dynamic behavior of boron carbide, J. Appl. Phys. **95**, 4173 (2004).

[39] P. Dera, M. H. Manghnani, A. Hushur, Y. Hu, and S. Tkachev, New insights into the enigma of boron carbide inverse molecular behavior, J. Solid State Chem. **215**, 85 (2014).

[40] A. Ektarawong, S. I. Simak, L. Hultman, J. Birch, F. Tasnádi, F. Wang, and B. Alling, Effects of configurational disorder on the elastic properties of icosahedral boron-rich alloys based on B_6O, $B_{13}C_2$, and B_4C, and their mixing thermodynamics, J. Chem. Phys. **144**, 134503 (2016).

[41] E. A. Ekimov, R. A. Sadykov, N. N. Mel'nik, A. Presz, E. V. Tat'yanin, V. N. Slesarev, and N. N. Kuzin, Diamond Crystallization in the System B_4C-C, Inorg. Mater. **40**, 932 (2004).

[42] E. A. Ekimov, V. A. Sidorov, R. A. Sadykov, N. N. Mel'nik, S. Gierlotka, and A. Presz, Synthesis of carbonado-like polycrystalline diamond in the B_4C-graphite system, Diamond Relat. Mater. **14**, 437 (2005).

[43] V. L. Solozhenko, O. O. Kurakevych, D. Andrault, Y. L. Godec, and M. Mezouar, Ultimate Metastable Solubility of Boron in Diamond: Synthesis of Superhard Diamondlike BC_5, Phys. Rev. Lett. **102**, 015506 (2009).

[44] P. V. Zinin, L. C. Ming, I. Kudryashov, N. Konoshi, M. H. Manghnani, and S. K. Sharma, Pressure- and temperature-induced phase transition in the B–C system, J. Appl. Phys. **100**, 013516 (2006).

[45] L. C. Ming, P. V. Zinin, X. R. Liu, Y. Nakamoto, and R. Jia, Synthesis of dense BC_x phases under high-pressure and high-temperature, J. Phys.: Conf. Ser. **215**, 012135 (2010).

[46] P. V. Zinin, L. C. Ming, H. A. Ishii, R. Jia, T. Acosta, and E. Hellebrand, Phase transition in BC_x system under high-pressure and high-temperature: Synthesis of cubic dense BC_3 nanostructured phase, J. Appl. Phys. **111**, 114905 (2012).

[47] V. L. Solozhenko, N. A. Dubrovinskaia, and L. S. Dubrovinsky, Synthesis of bulk superhard semiconducting B-C material, Appl. Phys. Lett. **85**, 1508 (2004).

[48] P. E. Blöchl, Projector augmented-wave method, Phys. Rev. B **50**, 17953 (1994).

[49] G. Kresse and J. Furthmüller, Efficiency of ab-initio total energy calculations for metals and semiconductors using a plane-wave basis set, Computat. Mater. Sci. **6**, 15 (1996).

[50] G. Kresse and J. Furthmüller, Efficient iterative schemes for *ab initio* total-energy calculations using a plane-wave basis set, Phys. Rev. B **54**, 11169 (1996).

[51] J. Perdew, K. Burke, and M. Ernzerhof, Generalized Gradient Approximation Made Simple, Phys. Rev. Lett. **77**, 3865 (1996).

[52] H. J. Monkhorst and J. D. Pack, Special points for Brillouin-zone integrations, Phys. Rev. B **13**, 5188 (1976).

[53] P. E. Blöchl, O. Jepsen, and O. K. Andersen, Improved tetrahedron method for Brillouin-zone integrations, Phys. Rev. B **49**, 16223 (1994).

[54] A. Togo and I. Tanaka, First principles phonon calculations in material science, Scr. Mater. **108**, 1 (2015).

[55] A. Togo, F. Oba, and I. Tanaka, First-principles calculations of the ferroelastic transition between rutile-type and $CaCl_2$-type SiO_2 at high pressures, Phys. Rev. B **78**, 134106 (2008).

[56] K. Parlinski, Z. Q. Li, and Y. Kawazoe, First-Principles Determination of the Soft Mode in Cubic ZrO_2, Phys. Rev. Lett. **78**, 4063 (1997).

[57] F. D. Murnaghan, On the theory of the tension of an elastic cylinder, Proc. Natl. Acad. Sci. USA **30**, 382 (1944).

[58] F. Birch, Finite Elastic Strain of Cubic Crystals, Phys. Rev. **71**, 809 (1947).

[59] R. Golesorkhtabar, P. Pavone, J. Spitaler, P. Puschnig, and C. Draxl, ElaStic: A tool for calculating second-order elastic constants from first principles, Comput. Phys. Commun. **184**, 1861 (2013).

[60] F. Tasnádi, M. Odén, and I. A. Abrikosov, *Ab initio* elastic tensor of cubic $Ti_{0.5}Al_{0.5}N$ alloys: Dependence of elastic constants on size and shape of the supercell model and their convergence, Phys. Rev. B **85**, 144112 (2012).

[61] J. F. Nye, *Physical Properties of Crystals: Their Representation by Tensors and Matrices* (Oxford University Press, Oxford, 1985).

[62] L. Vitos, *Computational Quantum Mechanics for Materials Engineers: The EMTO Method and Applications (Engineering Materials and Processes)* (Springer, Berlin, 2010).

[63] M. Moakher and A. N. Norris, The closest elastic tensor of arbitrary symmetry to an elasticity tensor of lower symmetry, J. Elast. **85**, 215 (2006).

[64] F. Mouhat and F.-X. Coudert, Necessary and sufficient elastic stability conditions in various crystal systems, Phys. Rev. B **90**, 224104 (2014).

[65] G. Simmons and H. Wang, *Single Crystal Elastic Constants and Calculated Aggregate Properties: A Handbook* (MIT Press, Cambridge, MA, 1971).

[66] H. Rydberg, M. Dion, N. Jacobson, E. Schröder, P. Hyldgaard, S. I. Simak, D. C. Langreth, and B. I. Lundqvist, Van der Waals Density Functional for Layered Structures, Phys. Rev. Lett. **91**, 126402 (2003).

[67] M. Dion, H. Rydberg, E. Schröder, D. C. Langreth, and B. I. Lundqvist, Van der Waals Density Functional for General Geometries, Phys. Rev. Lett. **92**, 246401 (2004).

[68] V. R. Cooper, Van der Waals density functional: An appropriate exchange functional, Phys. Rev. B **81**, 161104(R) (2010).

[69] K. Berland, V. R. Cooper, K. Lee, E. Schröder, T. Thonhauser, P. Hyldgaard, and B. I. Lundqvist, van der Waals forces in density functional theory: A review of the vdW-DF method, Rep. Prog. Phys. **78**, 066501 (2015).

[70] H. Shin, S. Kang, J. Koo, H. Lee, J. Kim, and Y. Kwon, Cohesion energetic of carbon allotropes: Quantum Monte Carlo study, J. Chem. Phys. **140**, 114702 (2014).

[71] A. R. Oganov, J. Chen, C. Gatti, Y. Ma, Y. Ma, C. W. Glass, Z. Liu, T. Yu, O. O. Kurakevych, and V. L. Solozhenko, Ionic high-pressure form of elemental boron, Nature (London) **457**, 863 (2009).

[72] E. Yu. Zarechnaya, L. Dubrovinsky, N. Dubrovinskaia, Y. Filinchuk, D. Chernyshov, V. Dmitriev, N. Miyajima, A. El Goresy, H. F. Braun, S. Van Smaalen, I. Kantor, A. Kantor, V. Prakapenka, M. Hanfland, A. S. Mikhaylushkin, I. A. Abrikosov, and S. I. Simak, Superhard Semiconducting Optically Transparent High Pressure Phase of Boron, Phys. Rev. Lett. **102**, 185501 (2009).

[73] M. P. Grumbach and R. M. Martin, Phase diagram of carbon at high pressures and temperatures, Phys. Rev. B **54**, 15730 (1996).

[74] L. M. Ghiringhelli, J. H. Los, E. J Meijer, A. Fasolino, and D. Frenkel, Modeling the Phase Diagram of Carbon, Phys. Rev. Lett. **94**, 145701 (2005).

[75] F. B. Bundy, W. A. Bassett, M. S. Weathers, R. J. Hemley, H. K. Mao, and A. F. Goncharov, The pressure-temperature phase and transformation diagram for carbon; updated through 1994, Carbon **34**, 141 (1996).

[76] M. M. Balakrishnarajan, P. D. Pancharatna, and R. Hoffmann, Structure and bonding in boron carbide: The invisibility of imperfections, New J. Chem. **31**, 473 (2007).

[77] J. H. Gieske, T. L. Aselage, and D. Emin, in *Elastic Properties of Boron Carbides*, AIP Conf. Proc. No. 231 (AIP, New York, 1991), p. 376.

[78] M. H. Manghnani, Y. Wang, F. Li, P. Zinin, and W. Rafaniello, Elastic and vibrational properties of B_4C to 21 GPa, Sci. Technol. High Press. **2**, 25 (2000).

[79] H. C. Longuet-Higgins and M. de V. Roberts, The electronic structure of an icosahedron of boron atoms, Proc. R. Soc. A **230**, 110 (1955).

[80] X. Guo, J. He, Z. Liu, Y. Tian, J. Sun, and H. T. Wang, Bond ionicities and hardness of $B_{13}C_2$-like structured B_yX crystals (X=C, N, O, P, As), Phys. Rev. B **73**, 104115 (2006).

[81] S. Aydin and M. Simsek, Hypothetically superhard boron carbide structures with a $B_{11}C$ icosahedral and three-atom chain, Phys. Status Solidi B **246**, 62 (2009).

[82] V. Domnich, Y. Gogotsi, M. Trenary, and T. Tanaka, Nanoindentation and Raman spectroscopy studies of boron carbide single crystals, Appl. Phys. Lett. **81**, 3783 (2002).

[83] K. Niihara, A. Nakahira, and T. Hirai, The effect of stoichiometry on mechanical properties of boron carbide, J. Am. Ceram. Soc. **67**, C-13 (1984).

[84] R. D. Allen, The solid solution series, boron-boron carbide, J. Am. Chem. Soc. **75**, 3582 (1953).

[85] M. A. Kuzenkova, P. S. Kislyi, B. L. Grabchuk, and N. I. Bodnaruk, The structure and properties of sintered boron carbide, J. Less-Common Met. **67**, 217 (1979).

[86] R. Raucoules, N. Vast, E. Betranhandy, and J. Sjakste, Mechanical properties of icosahedral boron carbide explained from first principles, Phys. Rev. B **84**, 014112 (2011).

[87] F. Izumi and K. Momma, Three-dimensional visualization in powder diffraction, Solid State Phenom. **130**, 15 (2007).

[88] K. Momma and F. Izumi, *VESTA3* for three-dimensional visualization of crystal, volumetric and morphology data, J. Appl. Crystallogr. **44**, 1272 (2011).